Stokes parameter studies of spontaneous emission from chiral nematic liquid crystals as a one-dimensional photonic stopband crystal: Experiment and theory

Kai L. Woon and Mary O'Neill*
Department of Physics, University of Hull, Cottingham Road, Hull, HU6 7RX, United Kingdom

Gary J. Richards, Matthew P. Aldred, and Stephen M. Kelly
Department of Chemistry, University of Hull, Cottingham Road, Hull, HU6 7RX, United Kingdom
(Received 8 October 2004; published 29 April 2005)

The helical structure of uniformly aligned chiral nematic liquid crystals results in a photonic stopband for only one sense of circular polarization. The spectroscopic Stokes polarimeter is used to analyze spontaneous emission in the stopband. Highly polarized photoluminescence is found and the polarization properties vary with the excitation wavelength. Spontaneous emission is enhanced at the stopband edge and this Purcell effect is greater on excitation at wavelengths where the absorption coefficient is low. This is interpreted as greater overlap between the excited molecules and the electrical modal field of the resonant modes at the stopband edge. Photoluminescence detected from the excitation face of the liquid crystal cell is less polarized because of photon tunneling. Fermi's golden rule in conjunction with Stokes vectors is used to model the polarization of emission taking multiple reflections at the interfaces of the cell into account. The discrepancy between the experiment and the theoretical model is interpreted as direct experimental evidence that virtual photons, which originate from zero point fluctuations of quantum space, are randomly polarized.

DOI: 10.1103/PhysRevE.71.041706 PACS number(s): 42.70.Df, 78.55.−m, 42.70.Qs, 83.80.Xz

I. INTRODUCTION

Spontaneous emission is not an intrinsic atomic property but rather results from the coupling of the atom to the vacuum modes of the electromagnetic field [1,2]. Spontaneous emission from an excited electronic state reflects the properties of the surrounding zero point fluctuations. The emission from an emitter in a microcavity can be suppressed [3] or enhanced [4] as a result of modification of the zero point fluctuation density inside the cavity compared to that of free space. The enhancement of spontaneous emission due to the cavity effect is called the Purcell effect. Experimental and theoretical studies have shown how the anisotropy of the vacuum fluctuation distribution inside a microcavity influences spontaneous emission [5,6]. Recent interest in microcavities and photonic crystals (PCs) is based on their technological potential in low threshold lasing and quantum information processing [7].

Chiral nematic liquid crystals (CNLCs) adopt a helical structure of period p and are considered one-dimensional (1D) PCs. Unlike other PCs [8], the photonic band gap of a CNLC is polarization dependent. When the liquid crystal is sandwiched in a planar texture, it forms a 1D Fabry-Pérot stopband. Circularly polarized light having the same handedness as the helix is selectively reflected when the optical wavelength matches the helical period. Inside the stopband the spontaneous emission of circularly polarized light having the same handedness as the helix is suppressed while at the stopband edge the emission is enhanced. Since the photonic stopband only occurs along the helical axis of CNLCs, the coupling of atoms to the vacuum modes of the electromagnetic field is weak.

In the weak coupling regime, the rate of spontaneous emission is described by Fermi's golden rule [9] given as

$$W_{i\to m} = \frac{2\pi}{\hbar}\left|\langle \Psi_m | \mu \cdot e(\omega_0, r_0) | \Psi_i \rangle\right|^2 \rho(E_m), \tag{1}$$

where $\rho(E_m)$ is the density of states (DOS) of photon energy E_m. μ is the electric dipole operator and $e(\omega_0, r_0)$, the electric modal field, is both a function of angular frequency ω_0 and position r_0. Ψ is the wave function of the electron making the transition from state i to m.

Very often the guest-host system, consisting of a low concentration of a laser dye in a host CNLC, is used to generate circularly polarized emission and band-edge lasing [10–15]. A theoretical model was developed by Schmidtke *et al.* to qualitatively account for the observed suppression and enhancement of circularly polarized emission [16]. However, it does not explain the excitation wavelength dependence of both suppression and enhancement of spontaneous emission. In this paper, an improved model is presented in Sec. II retaining the assumption that the spontaneous emission can be resolved independently for each eigenmode of propagation in CNLCs. We describe briefly the experimental setup in Sec. III. Then we present the experimental results and a qualitative interpretation. A theoretical model based on Fermi's golden rule is used to fit the experimental data in Sec. IV. We show that the polarization states of the emission depend on whether the light is detected from the excitation or rear side of the CNLC. The variation of the polarization of emission with excitation wavelength is also explained. We show that the divergence from orthogonality of the eigenmodes limits the agreement between theory and experiment when there is a large refractive index mismatch between the liquid crystals and the alignment layers.

*Electronic address: m.oneill@hull.ac.uk

 ©2005 The American Physical Society

II. THEORETICAL MODEL

A. Electromagnetic wave polarization and propagation inside the CNLC

In a monodomain planar aligned CNLC, the periodic modulation of the refractive index modifies the dispersion relationship of electromagnetic wave propagation so that the effective wave number k along the helix is given by [17,18]

$$k^2 = k_1^2 = \beta k_0^2 + q^2 - \sqrt{4q^2\beta k_0^2 + \alpha^2 k_0^4},$$

$$k^2 = k_2^2 = \beta k_0^2 + q^2 + \sqrt{4q^2\beta k_0^2 + \alpha^2 k_0^4}, \tag{2}$$

where k_0 is the wave number in vacuum, $\alpha = \frac{1}{2}(n_e^2 - n_0^2)$, $\beta = \frac{1}{2}(n_e^2 + n_0^2)$, and $q = 2\pi/p$, where p is the pitch of the CNLC. k_1 and k_2 are the two independent eigenmodes of propagation and n_e and n_o are the refractive indices for light polarized parallel and perpendicular to the director, respectively. The polarization of these basis waves under the rotating coordinate (ξ and η are the axes perpendicular and parallel to the local director of chiral nematic molecule, respectively) is given by

$$\hat{E}_{\xi\eta} = \begin{pmatrix} E_\xi \\ E_\eta \end{pmatrix} = \frac{1}{\sqrt{1 + |f|^2}} \begin{pmatrix} 1 \\ if \end{pmatrix}, \tag{3}$$

where

$$f = \frac{1 + a/b}{1 - a/b} \tag{4}$$

and

$$\frac{a}{b} = \frac{\alpha k_0^2}{(k - q)^2 - \beta k_0^2}. \tag{5}$$

One interesting property of light polarization inside the CNLC is that the eigenmode k_1 becomes imaginary in the stopband and is linearly polarized parallel to η at the red end of the stopband and perpendicular to it at the blue end of the stopband. Outside the stopband, the eigenmode k_1 is elliptically polarized with its major axis parallel to the local dielectric tensor director outside the red end of the stopband and perpendicular to it outside the blue end of the stopband. Less importantly, the eigenmode k_2 is elliptically polarized with opposite handedness with k_1 and the major axis of eigenmode k_2 is parallel to η [16,18].

B. Density of states

To calculate the rate of spontaneous emission we assume that the emission can be resolved into two independent propagating eigenmodes inside the CNLC. We do not assume refractive index matching between the CNLC and the polyimide. The density of photonic states ρ of a 1D Fabry-Pérot PC is the inverse of the group velocity and is given by [19,20]

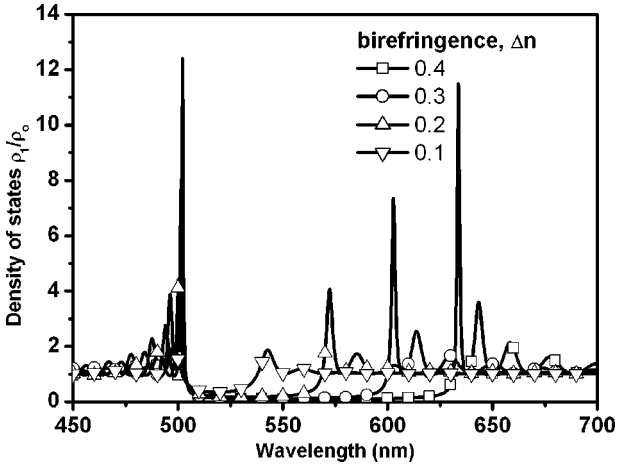

FIG. 1. Theoretical simulation of the DOS versus the birefringence for a CNLC cell with $n_o = 1.55$, $n_{\text{poly}} = 1.7$, $p = 325$ nm, and $L = 15p$.

$$\rho(\omega) \equiv \frac{dk}{d\omega} = \frac{1}{L}\frac{\dfrac{dy}{d\omega}x - \dfrac{dx}{d\omega}y}{x^2 + y^2}, \tag{6}$$

where L is the thickness of the PC and x and y are the real and imaginary parts of the transmission coefficients, respectively, at normal incidence. By considering the continuity relationship between two interfaces and Fabry-Pérot étalon-like multiple reflections, the DOS can be calculated for each eigenmode. Since we are concerned with its modification by the cavity and the distributed feedback structure, the DOS is scaled with respect to that, ρ_{iso}, of an infinite homogenous slab of constant refractive index. The scaled DOS is

$$\frac{\rho(\omega)}{\rho_{\text{iso}}} = \frac{\dfrac{dk}{d\omega}c}{\sqrt{\beta}}. \tag{7}$$

Figure 1 shows the change of the DOS with respect to birefringence for a CNLC cell of constant thickness. The resonant peaks observed at the stopband edges result from the constructive interference of light traveling back and forth between the two boundaries: peaks are created for light of effective wave number k when

$$kL = m\pi, \tag{8}$$

where m is an integer. The first resonant mode nearest to the stopband edge has the highest DOS and the slowest group velocity. This means that the interaction time between the radiation field and the excited atoms is the longest. Hence, the threshold for lasing at the first resonant mode is lowest as demonstrated by many authors [10,12–15]. As shown in Fig. 1 the DOS of the resonant peak increases with birefringence. The increase of the latter with material birefringence can be fitted by an exponential curve. Experimentally the lasing threshold is observed to exponentially decrease with increasing material birefringence at the first resonant mode [21].

C. Electric modal field

The rate of spontaneous emission depends on the location of the excited atom with respect to the electric modal field. The solution of the 1D Helmholtz wave equation has a general electric modal field inside the crystal with boundary conditions given by

$$E_m(z) = Af^+(z) + Bg^-(z), \tag{9}$$

where A and B are constants to be found and $f^+(z)$ and $g^-(z)$ are functions that depend on the refractive index. The superscript $+$ and $-$ signs indicate the forward and the backward propagating waves, respectively. If $n(z)$ is constant, then $f(z)$ and $g(z)$ are simple cosine and sine functions. For a wave of unit intensity in a linear system with no loss, A and B are given by [20]

$$A = \frac{Tg^-(0) - (1+R)g^-(L)}{f^+(L)g^-(0) - f^+(0)g^-(L)},$$
$$B = \frac{(1+R)f^+(d) - Tf^+(0)}{f^+(L)g^-(0) - f^+(0)g^-(L)}, \tag{10}$$

where R and T are the reflection and transmission coefficients for light traveling from the substrate to the PC, respectively. The electric modal field obtained is normalized with respect to the total energy. Unlike other 1D PCs, the electric modal field inside the CNLC is polarized. Using the ξ-η coordinate system, and noting that n_ξ and n_η are both constants, the electric modal field is

$$E(k,z) = E_{\xi\eta}E_m(z) = \frac{1}{\sqrt{1+|f|^2}}\begin{pmatrix}1\\ if\end{pmatrix}[A\sin(kz) + B\cos(kz)]. \tag{11}$$

Equation (11) describes both the polarization and the amplitude of the electrical model field of each eigenmode mode. The refractive index has the effect of concentrating the electric field, so that the electric modal field must be normalized with respect to the total field energy. Special care is taken to consider the anisotropy of the material. The electric energy density stored in an anisotropic material is given as

$$U = \left(\frac{1}{2}\hat{E}_{\xi\eta}\cdot D\right)E_m(z), \tag{12}$$

where D is the electric displacement vector given as

$$D = \varepsilon_{\text{local}}\cdot\hat{E}_{\xi\eta}, \tag{13}$$

and $\varepsilon_{\text{local}}$ is the local dielectric tensor of the CNLCs.

Using Eqs. (11)–(13), the total electric energy is

$$U = \frac{1}{2(1+|f|^2)}\int_0^L (n_0^2 + |f|^2 n_e^2)[|A\sin(kz) + B\cos(kz)|^2]dz. \tag{14}$$

Hence, the normalized electric modal field is

$$e(k,z) = \frac{E(k,z)}{\sqrt{U(k)}}. \tag{15}$$

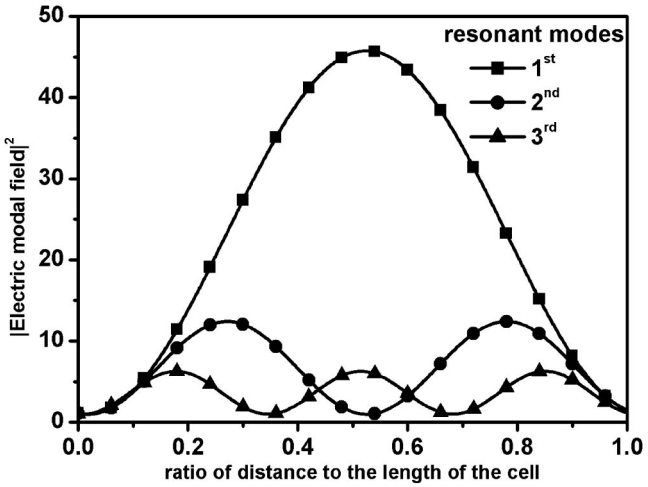

FIG. 2. The spatial dependence of $|\text{electric modal field}|^2$ for different resonances of the eigenmode k_1 at the stopband edge.

Figure 2 illustrates the spatial dependence of the electric modal field for the first three resonances of eigenmode k_1 from the stopband edge. For the first mode the probability of spontaneous emission is maximized in the center of the cell.

D. Orientation of dipole moment on spontaneous emission

As Eq. (1) shows, the spontaneous emission rate depends on the components of electric modal field along the electric transition dipole moment of the emitter. Hence the ordering and the shape of the dye influence the polarization and lasing threshold of the guest-host system [22,23]. The effect of the transition dipole moment has been clearly illustrated theoretically by Schmidtke *et al.* [16] with

$$\langle|d|^2\rangle = \langle|\hat{\mu}\cdot\hat{E}_{\eta\xi}|^2\rangle = \frac{2}{3}\frac{|f|^2 - 1/2}{|f|^2+1}S_d + \frac{1}{3}, \tag{16}$$

where S_d is the pseudo order parameter of the dipole moment. $S_d=1$ corresponds to perfect alignment of the electric transition dipole moment with the local director. $S_d=0.25$ corresponds to an isotropic orientation distribution while $S_d=-0.5$ corresponds to the perfect orientation perpendicular to the local director.

E. Influence of material absorption coefficient

The scaled spontaneous emission rate p is now given as

$$p(\lambda,z) = \frac{\rho(\omega)}{\rho_{\text{iso}}}\frac{|\hat{\mu}\cdot\hat{E}_{\xi\eta}E_m(z)|^2}{U(k)} = \frac{\rho(\omega)}{\rho_{\text{iso}}}\frac{\langle|d|^2\rangle|E_m(z)|^2}{U(k)}. \tag{17}$$

It is important to note that p is a function of distance and wavelength (we omit other constants associated with it). Equation (17) specifies the scaled spontaneous emission rate at a given point and wavelength inside the liquid crystals. The emitter has a finite absorption length so that the number of excited chromophores varies with distance. Let the ab-

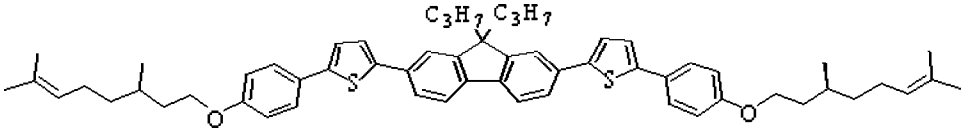

FIG. 3. The chemical structures of compound **a**.

sorption coefficient be α; the spatially integrated spontaneous emission rate $I_T(\lambda)$ is

$$I_T(\lambda) = \int_0^L p(\lambda,z)e^{-\alpha z}dz; \tag{18}$$

$I_T(\lambda)$ is the scaling factor used to describe the effect of the cavity on the intensity of the total photoluminescence detected along the helical axis.

F. Change of polarization upon propagating through polyimide/indium tin oxide/glass/air interfaces

In reality the transmitted electric fields have to propagate through a certain thickness of polyimide and indium tin oxide (ITO) and glass. The polarization of the light changes as it propagates through these layers as coherent reflection occurs at the interfaces of ITO and polyimide. We can ignore this effect since it does not change the degree of polarization, although the shapes of s_1/s_0 and s_2/s_0 are altered. We know that the degree of polarization is significantly reduced by rereflection at the glass-air interface [24]. We take this effect into account in this model using the Berreman transfer matrix where the reflection coefficient of the cell while traversing glass/ITO/polyimide/CNLC can be calculated. Since Jones vectors usually describe coherent light, the addition of two independent eigenmodes of spontaneous emission using Jones vectors would give an incorrect answer. However, if two separate beams of light are superposed incoherently, then the Stokes vector of the combination is simply the sum of the Stokes vectors of the original beams [25]. Hence, we use the Stokes parameters to characterize the polarization of light experimentally and theoretically. The Stokes parameters are defined as [26]

$$\begin{aligned} s_0 &= \langle E_{0x}^2 \rangle + \langle E_{0y}^2 \rangle, \\ s_1 &= \langle E_{0x}^2 \rangle - \langle E_{0y}^2 \rangle, \\ s_2 &= 2\langle E_{0x}E_{0y} \cos \delta \rangle, \\ s_3 &= 2\langle E_{0x}E_{0y} \sin \delta \rangle, \end{aligned} \tag{19}$$

where E_{0x} and E_{0y} are the electric field amplitudes along the x and y axes, respectively, and δ is the phase difference. It is evident that s_0 is the total intensity of the light while s_1 measures the intensity difference between light polarized parallel to x and y, respectively. s_2 is the difference in intensity between polarized light at angles of $-\pi/4$ and $\pi/4$. s_3 presents the difference in intensity between right and left circularly polarized light. The polarization of emission of each eigenmode obtained from the model has to be transformed into Stokes vectors before adding them incoherently. This method has proved to be useful in modeling the transmission of unpolarized light through CNLCs [24].

III. EXPERIMENT

Figure 3 shows the chemical structure of the liquid crystal **a** used in this work. On cooling from the chiral nematic phase, compound **a** forms a nematic glass with a glass transition temperature of 29 °C. A commercial cell of cell gap 5 μm having indium tin oxide substrates coated with rubbed polyimide alignment layers is filled with compound **a**. We have previously shown that the spontaneous emission from **a** is highly polarized with a maximum circular extinction ratio of 16:1 [27]. The spectroscopic Stokes polarimeter is calibrated [24], and used to characterize the polarization state of emission. The refractive indices are measured using a simple interference method described elsewhere [28]. n_e varies from 2.28 at 450 nm to 1.83 at 600 nm while n_0 is 1.63 independent of wavelength considered in this experiment (540–700 nm). It has a helical pitch of 288 nm when filled in a 5 μm cell to give a stopband from 470 to 578 nm. A depolarized laser is used to excite the sample.

IV. RESULTS AND DISCUSSION

A. Experimental results

I_L and I_R are the intensities detected when photoluminescence (PL) passes through a quarter wave plate followed by an analyzer set at $+45°$ and $-45°$ from its fast axis, respectively. Although they are often used to find the degree of circular polarization through a CNLC [11,14], I_L and I_R do not necessarily describe left and right circularly polarized light but can contain linear and unpolarized as well as circularly polarized components. Figure 4 shows I_L and I_R following excitation at a wavelength of (a) 405 and (b) 458 nm, respectively, and detected from the opposite face of the cell

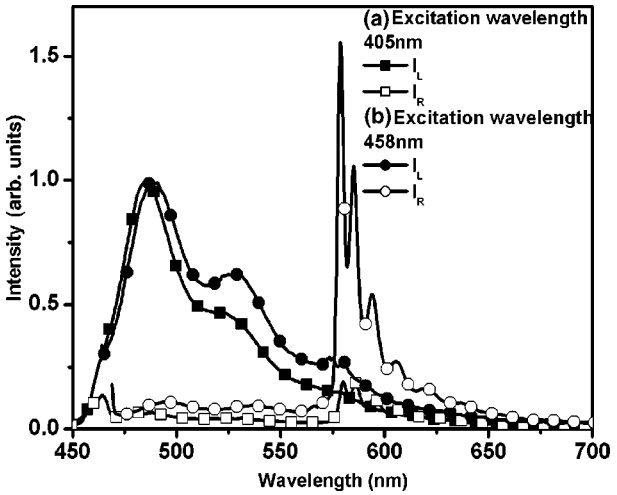

FIG. 4. I_L and I_R as a function of wavelength for excitation at (a) 405 and (b) 458 nm, respectively. The light is detected from the opposite face of the cell to the excitation beam.

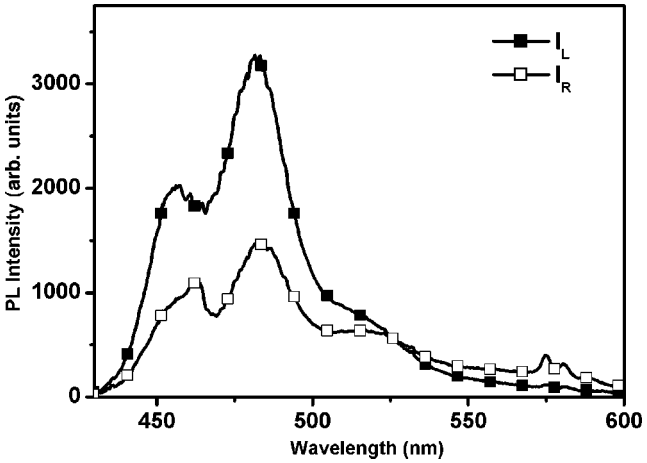

FIG. 5. I_L and I_R detected from the same face of the cell as the excitation beam of wavelength 405 nm.

to the excitation beam. Figure 5 shows the PL components detected from the same face of the cell as the excitation beam of wavelength 405 nm. The spectra for both I_L and I_R depend on excitation wavelength and detection geometry. For 405 nm excitation the emission is highly polarized with a maximum value of I_L/I_R of 16:1 at 536 nm. The apparent dependence of the Purcell effect on excitation wavelength is related to different absorption lengths at the two different excitation wavelengths. As Fig. 6 shows, the electric field of the excitation beam at 405 nm is confined to a relatively thin layer ~ 0.3 μm. The longer wavelength excitation penetrates deeper into the liquid crystal cell, providing a greater overlap with the electric modal field of the resonant modes at the stopband edge. Hence emission of the resonant modes is enhanced for I_R as shown in Fig. 4(b). Figure 4(a) shows a larger suppression of I_R inside the stopband compared with that shown in both Figs. 4(b) and 5. In both the latter cases molecules are excited near the detection side of the cell and the larger I_R is interpreted as photon tunneling where the emitters near the detection side of the cell "sense" a shorter photonic crystal. This result is confirmed theoretically: Fig. 7 shows the wavelength dependence of the ratio $I_{T1}:I_{T2}$, where

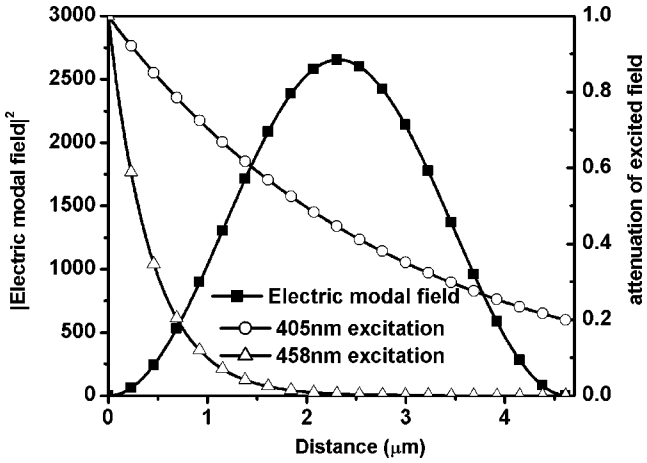

FIG. 6. The coupling of first resonant electric modal field with the excitation species at 405 and 458 nm.

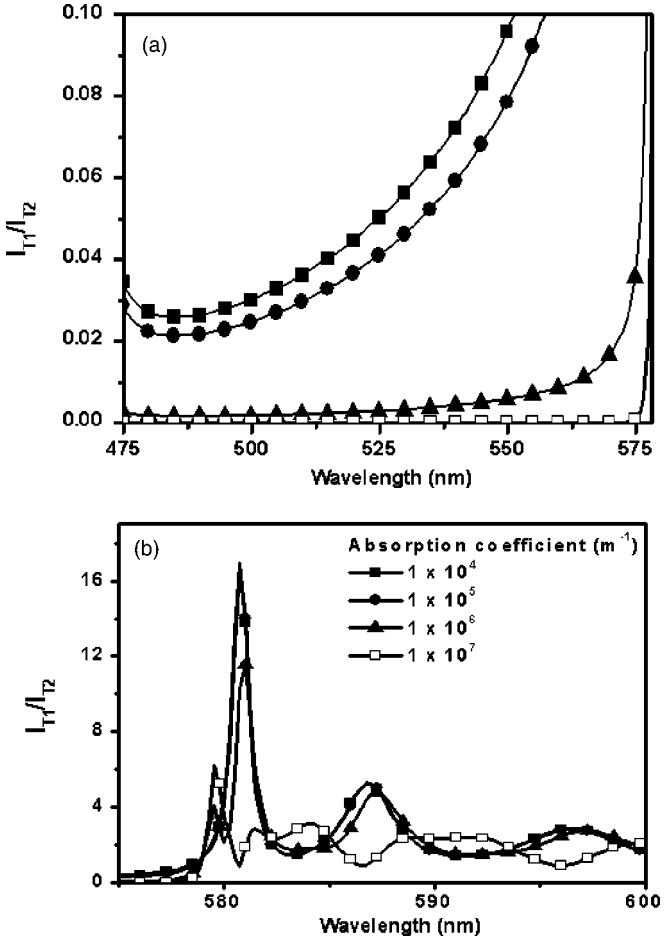

FIG. 7. The wavelength dependence of the ratio of the normal modes of emission (a) inside the stopband and (b) around the stopband edge.

the subscripts refer to spatially integrated spontaneous emission rates for eigenmodes 1 and 2, respectively, (a) inside and (b) outside the stopband for different absorption coefficients. An increase in absorption coefficient results in a larger suppression and a smaller enhancement of I_{T1} inside and outside the stopband, respectively.

B. Stokes parameter analysis: Experiment and theory

We now compare the theoretical simulations of the polarization states of PL with the experimental data. We take $S_d = 0.83$ for compound **a** as a nematic compound with the same core as **a** gives polarized electroluminescence with a linear polarization ratio of 11:1 [29]. This is related to the degree of orientation of the electric transition dipole moment by

$$S = \frac{I_{11} - I_{\perp}}{I_{11} + 2I_{\perp}} \leqslant S_d. \tag{20}$$

The theoretical simulation uses a spectral resolution of 0.25 nm and the simulated results are then averaged over eight points to obtain a resolution of 2 nm, equal to that obtained experimentally. Figure 8(a) shows the experimental and theoretical values of s_3/s_0 as a function of wavelength for excitation at 458 nm. Although the spectra are similar, the theory

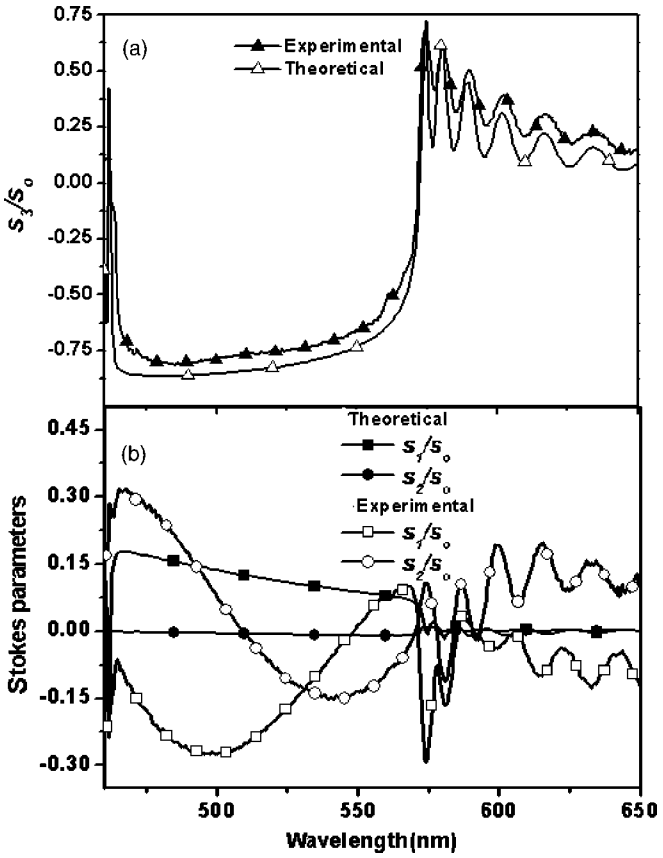

FIG. 8. Theoretical and experimental values of (a) s_3/s_0 and (b) s_1/s_0 and s_2/s_0 as a function of wavelength for excitation at 458 nm. $\alpha=2.3\times10^4$ m^{-1}, $p=284$ nm.

predicts a greater degree of circularly polarized emission than is obtained in the stopband and a lower degree outside the stopband. Figure 8(b) shows the experimental and theoretical results for s_1/s_0 and s_2/s_0 for the same excitation conditions. In this case the theory and experimental data have completely different spectra. Using a Stokes analysis, we have previously shown that the mismatch of refractive index between the liquid crystal and polyimide results in linear polarized components in the transmitted light [24]. It is not surprising to find such polarization states in PL. The change of polarization when the light propagates through the polyimide-ITO-glass layer is not included in the simulations so the theoretical values of s_1/s_0 and s_2/s_0 are not expected to quantitatively agree with the experimental results. However, given the refractive index mismatch, it is surprising that the theoretical simulation of s_2/s_0 is approximately zero in the stopband. Figure 9 shows the s_1/s_0 and s_2/s_0 components obtained from PL excited by 405 nm laser and from transmission of incident *unpolarized* light through the cell. It is clear that they have similar spectra. However, unlike the PL data, the experimental values of s_1/s_0 and s_2/s_0 in transmission agree closely with the calculated values [24].

The degree of polarization is unaffected by the omission of ITO in the theoretical modeling and hence provides a better parameter to compare theory with experiment. Figure 10 shows the result for (a) 458 and (b) 405 nm excitation. The difference between the experiment and theory is significant with the theory consistently overestimating the degree of polarization in the stopband. For 405 nm excitation, the theory predicts a degree of polarization for PL into the rear glass substrate of ≈100%. Rereflection of light at the glass-air interface of the cell results in a reduction to 92% in the degree of polarization of the detected PL.

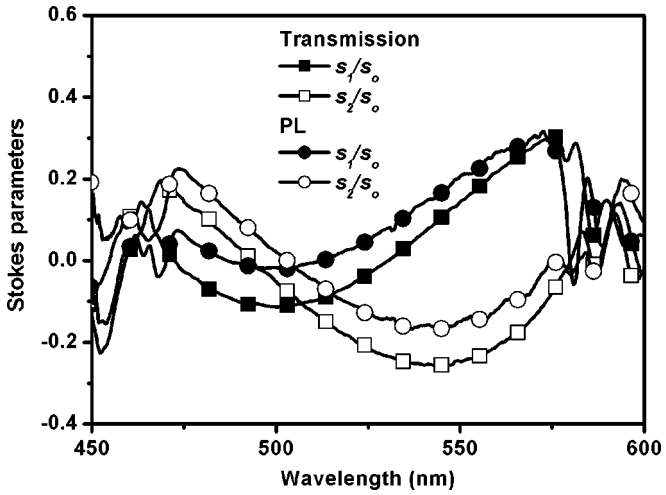

FIG. 9. Experimental values of s_1/s_0 and s_2/s_0 as a function of wavelength obtained for PL following excitation at 405 nm and transmission of unpolarized light through the cell.

We now examine the reasons for the discrepancy between theory and experiment. Incoherent right and left circularly

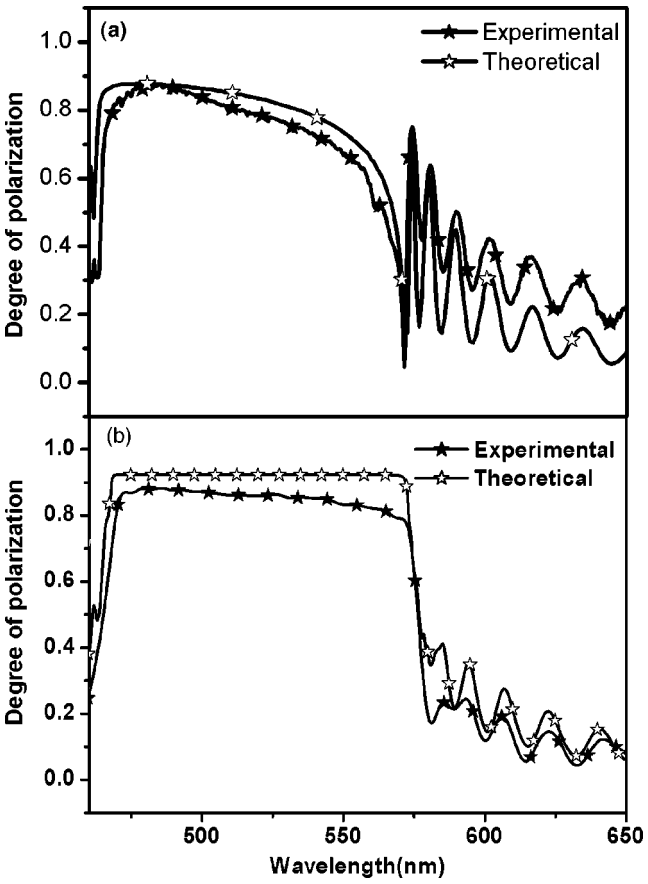

FIG. 10. Comparison of degree of polarization between experimental and theoretical results for (a) 458 and (b) 405 nm excitation.

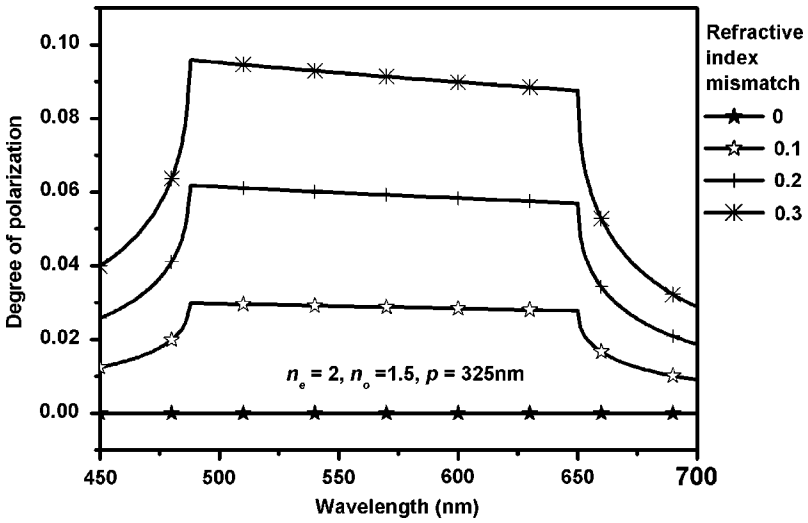

FIG. 11. The degree of polarization of the incoherently summed incident waves, used to calculate the two independent eigenmodes of emission, for different values of refractive index mismatch between liquid crystal and substrate.

polarized light is used as basis states in the transmission model to simulate the incident unpolarized light. According to quantum field theory, spontaneous emission results from the coupling of excited molecules to virtual photons that form the zero point fluctuations. The PL model assumes that the electric modal field can be resolved into two independent eigenmodes of propagation. In the transmission experiment the interaction of the CNLC Fabry-Pérot cavity with the external unpolarized light creates propagating modes within the cavity. Similarly, the same pattern should be established in PL by the virtual photons which must obey Maxwell equations. Since it is possible to interpret spontaneous emission as stimulated emission due to quantum fluctuations [30], we should expect similarity of the state of polarization of virtual photons with the state of polarization of spontaneous emission perturbed by the virtual photons. PL excited at 405 rather than 458 nm is used to compare with transmission because the emission is essentially restricted to a thin layer and hence the magnitude of electrical modal field is almost constant across the wavelength range considered. The electrical modal field inside the photonic crystal cavity and its polarization are established by unpolarized virtual photons from its immersive surrounding. The immersive surrounding is isotropic and hence corresponds to the vacuum modes of virtual photons. The similarity in the wavelength dependence in the stopband for transmission and PL indicates that the virtual photons of the vacuum modes are indeed randomly polarized. We now check whether the incoherent superposition of light that produces the eigenmodes used as basis states in PL gives unpolarized light. The two incident polarized waves that result in the two independent eigenmodes are calculated and transformed into Stoke parameters to be incoherently summed. Figure 11 shows the wavelength dependence of the degree of polarization of the resultant wave as a function of the refractive index mismatch between the liquid crystal and the polyimide. The incoherently summed waves are unpolarized when the refractive index of the substrate is matched to $\sqrt{\beta}$ of the CNLCs but become more polarized as the refractive index mismatch is increased and so do not accurately describe the vacuum field. Therefore the theoretical description of spontaneous emission in terms of two independent propagating eigenmodes is only an approximation when there is a refractive index mismatch. The difference between the two approaches is small when the refractive index mismatch of the CNLC is small but is significant for our system where there is a large refractive index mismatch. Our results show that the virtual photons that originate from the zero point fluctuations are unpolarized. This is supported by a study of the classical electromagnetic zero point field as an analogy for the vacuum of quantum field theory. The probability distribution for an unbounded zero point field is found to be isotropic where the polarization vector distribution is equally possible for all polarizations [31].

V. CONCLUSIONS

We have demonstrated highly circularly polarized photoluminescence from compound **a** exhibiting the widest stopband known in a pure chiral nematic liquid crystal. The stopband, which exists for one state of polarization only, almost completely overlaps the emission spectrum of compound **a** giving a very high degree of polarization over 110 nm. We demonstrate the usefulness of the spectroscopic Stokes polarimeter in studying the polarization of light from photonic crystals. PL detected from the same face of the cell as the incident excitation beam is less well polarized in the stopband since the forbidden mode is less well suppressed because of photon tunneling. The polarization properties of PL depend on the absorption coefficient and hence the excitation wavelength: the Purcell effect is enhanced when the absorption coefficient is low because the spatial distribution of excited molecules is better coupled to the resonant modes at the stopband edge. Fermi's golden rule is used to theoretically model the Stokes parameters and degree of polarization of PL from uniformly aligned compound **a**. The theoretical and experimental results do not agree quantitatively. We show that the assumption that spontaneous emission can be resolved into two independent eigenmodes derived from De Vries theory becomes less valid with increasing refractive index mismatch. We suggest that the invalidity of the assumption results directly from the existence of randomly polarized virtual photons.

[1] H. Yokoyama and K. Ujihara, *Spontaneous Emission and Laser Oscillation in Microcavities* (CRC Press, Boca Raton, FL, 1995), pp. 2–4.
[2] H. B. Callen and T. A. Welton, Phys. Rev. **83**, 34 (1951).
[3] E. M. Purcell, Phys. Rev. **69**, 681 (1946).
[4] D. Kleppner, Phys. Rev. Lett. **47**, 233 (1981).
[5] I. Takahashi and K. Ujihara, Phys. Rev. A **56**, 2299 (1997).
[6] S. M. Dutra and P. L. Knight, Phys. Rev. A **53**, 3587 (1996).
[7] M. H. Qi, E. Lidorikis, P. T. Rakich, S. G. Johnson, J. D. Joannopoulos, E. P. Ippen, and H. I. Smith, Nature (London) **429**, 538 (2004).
[8] J. D. Joannopoulos, R. D. Meade, and J. N. Winn, *Photonic Crystals* (Princeton University Press, Princeton, NJ, 1995).
[9] P. W. Atkins and R. S. Friedman, *Molecular Quantum Mechanics*, 3rd ed. (Oxford University Press, Oxford, 1997), pp. 193–195.
[10] J. Schmidtke, W. Stille, H. Finkelmann, and S. T. Kim, Adv. Mater. (Weinheim, Ger.) **14**, 746 (2002).
[11] S. H. Chen, D. Katsis, A. W. Schmid, J. C. Mastrangelo, T. Tsutsui, and T. N. Blanton, Nature (London) **397**, 506 (1999).
[12] V. I. Kopp, B. Fan, H. K. M. Vithana, and A. Z. Genack, Opt. Lett. **23**, 1707 (1998).
[13] V. I. Kopp, Z. Q. Zhang, and A. Z. Genack Phys. Rev. Lett. **86**, 1753 (2001).
[14] M. Voigt, M. Chambers, and M. Grell, Chem. Phys. Lett. **347**, 173 (2001).
[15] S. Furumi, S. Yokoyama, A. Otomo, and S. Mashiko, Thin Solid Films **438**, 423 (2003).
[16] J. Schmidtke and W. Stille, Eur. Phys. J. B **31**, 179 (2003).
[17] P. Yeh and C. Gu, *Optics of Liquid Crystal Displays* (John Wiley & Sons, New York, 1999), pp. 282–298.
[18] H. De Vries, Acta Crystallogr. **4**, 219 (1951).
[19] J. M. Bendickson, J. P. Dowling, and M. Scalora, Phys. Rev. E **53**, 4107 (1996).
[20] J. P. Dowling, J. Lightwave Technol. **17**, 2142 (1999).
[21] J. R. Willmott, in Abstracts of the British Liquid Crystal Conference, 2003 (unpublished).
[22] K. Bjorknas, E. P. Raynes, and S. Gilmour, J. Mater. Sci.: Mater. Electron. **14**, 397 (2003).
[23] F. Araoka, K.-C. Shin, Y. Takanishi, K. Ishikawa, H. Takezoe, Z. Zhu, and T. M. Swager, J. Appl. Phys. **94**, 279 (2003).
[24] K. L. Woon, M. O'Neill, P. Vlachos, M. P. Aldred, and S. M. Kelly, J. Opt. Soc. Am. A **22**, 760 (2005).
[25] R. C. Jones, J. Opt. Soc. Am. **37**, 107 (1947).
[26] M. Born and E. Wolf, *Principles of Optic* (Cambridge University Press, Cambridge, U.K., 1988), pp. 544–555.
[27] K. L. Woon, M. O'Neill, G. J. Richards, M. P. Aldred, S. M. Kelly, and A. M. Fox, Adv. Mater. (Weinheim, Ger.) **15**, 1555 (2003).
[28] K. L. Woon, M. O'Neill, P. Vlachos, M. P. Aldred, and S. M. Kelly (unpublished).
[29] A. E. A. Contoret, S. R. Farrar, P. O. Jackson, S. M. Khan, L. May, M. O'Neill, J. E. Nicholls, S. M. Kelly, and G. J. Richards, Adv. Mater. (Weinheim, Ger.) **12**, 971 (2000).
[30] Peter W. Milonni, *The Quantum Vacuum: An Introduction to Quantum Electrodynamics* (Academic Press, New York, 1993), pp. 20–25.
[31] M. Ibison and B. Haisch, Phys. Rev. A **54**, 2737 (1996).